IJMMM International Journal of Minerals, Metallurgy and Materials 矿物冶金与材料学报（英文版）

A simple and novel synthetic route to prepare anatase TiO_2 nanopowders from natural ilmenite via the H_3PO_4/NH_3 process

Lalinda Palliyaguru, Ushan S. Kulathunga, Lakruwani I. Jayarathna, Champa D. Jayaweera, and Pradeep M. Jayaweera

Cite this article as:
Lalinda Palliyaguru, Ushan S. Kulathunga, Lakruwani I. Jayarathna, Champa D. Jayaweera, and Pradeep M. Jayaweera, A simple and novel synthetic route to prepare anatase TiO_2 nanopowders from natural ilmenite via the H_3PO_4/NH_3 process, *Int. J. Miner. Metall. Mater.*, 27(2020), No. 6, pp. 846-855. https://doi.org/10.1007/s12613-020-2030-3

International Journal of Minerals, Metallurgy and Materials
Volume 27, Number 6, June 2020, Page 846
https://doi.org/10.1007/s12613-020-2030-3

A simple and novel synthetic route to prepare anatase TiO_2 nanopowders from natural ilmenite via the H_3PO_4/NH_3 process

Lalinda Palliyaguru, Ushan S. Kulathunga, Lakruwani I. Jayarathna, Champa D. Jayaweera, and Pradeep M. Jayaweera

Department of Chemistry, University of Sri Jayewardenepura, Nugegoda-10250, Sri Lanka
(Received: 3 October 2019; revised: 24 February 2020; accepted: 25 February 2020)

Abstract: A simple and novel technique for the preparation of anatase TiO_2 nanopowders using natural ilmenite ($FeTiO_3$) as the starting material is reported. Digesting ilmenite with concentrated H_3PO_4 under refluxing conditions yields a white α-titanium bismonohydrogen orthophosphate monohydrate (TOP), $Ti(HPO_4)_2{\cdot}H_2O$, which can be easily isolated via gravity separation from unreacted ilmenite. The addition of ammonia to the separated TOP followed by calcination at 500°C completes the preparation of anatase TiO_2. Calcination at temperatures above 800°C converts the anatase form of TiO_2 to the stable rutile phase. The removal of iron from ilmenite during the commercial production of synthetic TiO_2 is problematic and environmentally unfriendly. In the present study, the removal of iron was found to be markedly simple due to the high solubility of iron phosphate species in concentrated H_3PO_4 with the precipitation of TOP. The titanium content of the prepared samples on metal basis with silica and phosphorous as major impurities was over 90%. Prepared TiO_2 samples were characterized using X-ray fluorescence, Fourier-transform infrared spectroscopy, Raman spectroscopy, ultraviolet–visible diffuse reflectance spectroscopy, high-resolution transmission electron microscopy, and X-ray diffraction analyses. The photocatalytic potentials of the commercial and as-prepared TiO_2 samples were assessed by the photodegradation of rhodamine B dye.

Keywords: ilmenite; phosphoric acid; titanium phosphates; titanium dioxide; anatase; rutile

1. Introduction

TiO_2 is a mineral that occurs in nature as three well-known polymorphs: rutile, anatase, and brookite. Among the three polymorphs, rutile is the most abundant and stable phase [1–2]. Anatase and brookite are metastable phases that transform exothermally and irreversibly into rutile under heat, pressure, or other conditions. The phase transition [3–6] of anatase to rutile occurs in the temperature range of 350–1175°C and enables anatase to be used in technological applications. The crystal structures of rutile, anatase, and brookite are all based on distorted TiO_6 octahedral units that share corners and edges in different connections while keeping the overall stoichiometry as TiO_2. Rutile has a straight chain of octahedra linked via corner connections, and anatase has a zigzag chain of octahedra linked via edge connections. Anatase has more edge-sharing octahedra than rutile and therefore has larger interstitial spaces between the octahedra. The crystal structures of these polymorphs and other known physical properties, such as refractive index and density, are interconnected [5,7–8]. For example, rutile with a high refractive index makes it a superior pigment [9]. Anatase with a larger band gap makes it more photoactive than rutile. The high photoactivity of anatase thus facilitates its use in a number of applications involving solar cells and photocatalysis [10–11].

Of the many techniques used to prepare anatase TiO_2 nanomaterials [12–14], hydrothermal methods have gained much interest due to their relative simplicity, cost effectiveness, and varying degrees of chemical/physical properties [15–16]. According to previous work, titanium(IV) compounds, mainly but not exclusively $TiCl_4$, and organic titanium have been widely used as starting materials in the preparation of the anatase phase [12,14,17–18]. A number of groups have attempted to selectively crystallize anatase or rutile after the hydrolysis of $TiCl_4$ by controlling the solution pH, concentration of reactants, and mineralizers [5,19]. Parra *et al.* [20] prepared high-purity anatase nanoparticles with diameters ranging from 6 to 30 nm from titanium(IV) isopropoxide and acetic acid. Titanium alkoxide was successfully

Corresponding author: Pradeep M. Jayaweera E-mail: pradeep@sjp.ac.lk

used in the synthesis of anatase nanomaterials via sol–gel hydrolysis, precipitation, and calcination or hydrothermal treatment [18]. The precise control over these laboratory parameters is critical to phase selectivity. The high sensitivity of $TiCl_4$ and alkoxides to atmospheric moisture is a major disadvantage in the industrial production of anatase TiO_2.

Ilmenite ($FeTiO_3$) is the most abundant and most widely used material in the synthesis of titanium compounds, including anatase TiO_2, $TiCl_4$, and organic titanium [21–22]. The removal of iron, the major impurity in ilmenite, is challenging because of the large quantities of iron present in ores. This condition is primarily due to the lack of selectivity between iron and titanium in acid/base dissolution kinetics [21,23]. Currently, the sulfate and chloride processes are the two major industrial-scale processes available for the production of titanium compounds from ilmenite [24–25]. The main feedstocks for these processes are TiO_2 slag and/or synthetic rutile produced from ilmenite ores. The most common method for producing TiO_2 slag is via smelting, in which iron oxide is reduced to liquid iron in an electric arc furnace. TiO_2 can be used to produce synthetic rutile, which is a further upgraded raw material with a TiO_2 content of 92wt%–96wt%. The preparation of synthetic anatase from ilmenite ores involves several additional steps after the synthesis of pure titanium(IV) compounds. For example [26–27], recent attempts to prepare synthetic anatase via the digestion of ilmenite using two common leaching agents, namely, HCl and H_2SO_4, involved several physical and chemical processing steps. Physical processes include the calcination and mechanical activation of ilmenite prior to acid leaching, as well as the use of iron powder and other chemicals (e.g., Na_2S and H_2O_2). Hence, these processes are less commercially viable than chemical processes for the preparation of anatase TiO_2.

The present study reports a simple and novel hydrothermal method for the direct preparation of synthetic anatase from ilmenite through digestion with concentrated H_3PO_4 followed by the addition of ammonia. The use of ilmenite as the feedstock and the absence of additional steps in the iron removal process are the key advantages of this method over other synthetic routes for the synthesis of anatase TiO_2. In addition, the entire chemical process requires only two industrial chemicals and does not involve high energy steps, such as smelting. The solid precipitate of α-titanium bismonohydrogen orthophosphate monohydrate (TOP), $Ti(HPO_4)_2{\cdot}H_2O$, separated from soluble iron complexes after digestion in concentrated phosphoric acid solution was reacted with ammonia to obtain anatase TiO_2. It was recently reported [28] that the preparation of TOP, a white pigment from ilmenite, using 85wt% H_3PO_4 has possible applications in the cosmetic industry. In the present investigation, the same material was used as a precursor for the synthesis of anatase-grade TiO_2. Furthermore, rutile-phase TiO_2 was obtained upon the heat treatment of the prepared anatase. The photocatalytic activities of the as-prepared TiO_2 compounds on rhodamine B (RhB) were assessed and compared with those of commercial-grade TiO_2 samples.

2. Experimental

2.1. Preparation of anatase/rutile nanopowder

First, TOP was synthesized by digesting 100 g of Hi-Ti grade ilmenite (Lanka Mineral Sands Limited, Sri Lanka) and 800 mL of 85wt% H_3PO_4 (Orthophosphoric Acid LR, Techno Pharmchem, India) for 5 h under refluxing condition. The mixture was allowed to cool down and settle into layers at room temperature. A white precipitate of TOP was settled between the most dense layer of the unreacted ilmenite at the bottom and the least dense layer of the liquid portion rich with iron phosphates on top (Fig. 1). The two upper layers were separated mechanically via a decantation technique, and the unreacted ilmenite remained in the reaction vessel. The separated middle layer rich with TOP was thoroughly mixed with 100 mL of distilled water and allowed to resettle for 24 h. This step was repeated four times until the white portion became free of residual amounts of unreacted ilmenite and H_3PO_4. The identity of TOP was confirmed by X-ray diffraction (XRD) and Fourier-transform infrared (FTIR) analysis. Second, 500 mL of 25wt% NH_3 (Research Lab Fine Chem Industries, India) was added to 55 g of pure TOP, and the resulting mixture was vigorously stirred for 2 h at 40°C. This step was repeated four times, and the mixture was allowed to settle at room temperature for 24 h. The white precipitate was separated and calcined (box-type resistance furnace SX-2.5-10, China) at 500, 700, 800, and 900°C. The XRD pattern of the final product confirmed the formation of anatase. The ilmenite samples and all chemicals were used as received without any further purification.

2.2. XRD analysis

The XRD patterns of the ilmenite, TOP, anatase, and rutile samples were analyzed using an XRD instrument (Rigaku Ultima-IV) equipped with a Cu K_α source and scintillation detector. Diffractograms were generated by scanning in the 2θ range of 10°–100° with a 0.02° step size and a scan time of 1 s per step. The prepared TiO_2 samples were calcined for 5 h at the temperatures of 500, 700, 800, and 900°C prior to the XRD analysis. The particle diameters (D) of the prepared TiO_2 samples were calculated from the most intense diffraction peaks of (101) and (110) for the anatase and rutile, respectively, using the Scherrer formula (Eq. (1)) [29] given as

$$D = \frac{0.9\lambda}{\beta\cos\theta} \tag{1}$$

where λ is the X-ray wavelength employed, θ is the diffraction angle of the corresponding peak, and β is defined as the full-width at half maximum of the peak.

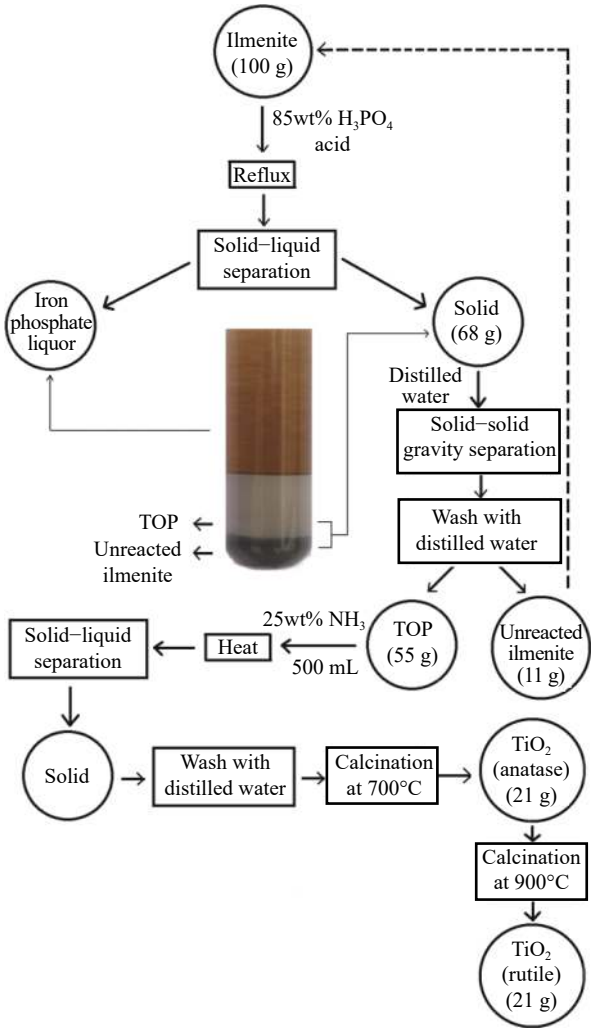

Fig. 1. Flowchart of the preparation of TiO_2 from ilmenite.

The weight percentage of anatase, x_A, was determined for each calcination temperature using the following Spurr equation [30]:

$$x_A = \frac{I_A}{I_A + 1.265 \times I_R} \times 100\% \quad (2)$$

where I_A and I_R correspond to the areas of the anatase (101) and rutile (110) XRD peaks, respectively. Therefore, the rutile percentage (x_R) was computed as $x_R = 1 - x_A$.

2.3. TEM analysis

The morphology of the powder materials was investigated by high-resolution transmission electron microscopy (HR-TEM, ZEISS Libra 200 Cs-TEM, Germany) at an accelerating voltage of 200 kV. The transmission electron microscopy (TEM) images of the TiO_2 samples were obtained after calcining them at 700 and 900°C. The particle sizes were analyzed using the ImageJ software.

2.4. Raman spectroscopy

The Raman spectra of the TiO_2 samples were obtained with a Bruker Senterra Raman spectrometer with a laser excitation wavelength of 785 nm and an incident power of 10 mW. The aperture size and integration time were respectively set to 25 μm × 1000 μm and 5 s during the data collection.

2.5. X-ray fluorescence (XRF) analysis

The chemical composition of the samples was analyzed by XRF using a HORIBA Scientific XGT-5200 X-ray analytical microscope equipped with an Rh anode X-ray tube operated at a maximum voltage of 50 kV and current of 1 mA with a Peltier-cooled silicon drift detector.

2.6. UV–Vis diffuse reflectance spectroscopy

The ultraviolet–visible diffuse reflectance spectra (UV–Vis DRS) of the powder samples were measured using a PerkinElmer Lambda 35 spectrometer. The UV–Vis DRS were obtained with a 31.75 mm calibrated certified reflectance standard (SRS-99-010) as the background equipped with a 50 mm integrating sphere. The optical reflectance was measured in the 300–900 nm range.

UV–Vis absorbance spectroscopy coupled with the Kubelka–Munk method [31] was used to evaluate the band gap energies of the prepared anatase and rutile TiO_2. The Kubelka–Munk method is based on the following equation:

$$F(R) = \frac{(1-R)^2}{2R} = \frac{\alpha}{s} \quad (3)$$

where $F(R)$ is the Kubelka–Munk function, R is the reflectance, s is the scattering factor, and α is the absorption coefficient. The modified Kubelka–Munk function can be expressed as follows:

$$[F(R) \times h\upsilon]^n \quad (4)$$

where n is associated with the electronic transition. $n = 1/2$ for an indirect allowed transition, and $n = 2$ for a direct allowed transition.

2.7. Photocatalytic degradation of rhodamine B

The photocatalytic activities of the prepared TiO_2 samples were tested by bleaching a sample of RhB (Loba Chemie, India) dissolved in 50.00 mL of distilled water under UV irradiation (250 W Hg arc Philips UV Lamp). In a typical experiment, a sample of 150.0 mL of dye solution loaded with 0.10 g of TiO_2 was exposed to UV light. All the photocatalytic tests were conducted by stirring the suspension with a magnetic stirrer. Before irradiation, all samples were stored in the dark for 20 min to make them reach the sorption equilibrium. After being illuminated for a certain period of time, a sample of the suspension was centrifuged at 5000 r/min for 20 min to achieve a clear separation of the liquid portion. The concentration of the RhB in the solution was determined through UV–Vis spectroscopy by measuring absorbance (Perkinelmer Lambda 35, USA) at 554 nm. A commercial anatase TiO_2 sample (Merck, K19722608) was

used for comparison. Pigment-grade TiO_2 (Brand Ti-Pure™, China) was used as the commercial rutile.

3. Results and discussion

3.1. Preparation of anatase/rutile TiO_2

The flowchart for the preparation of anatase/rutile TiO_2 from the starting material ilmenite is shown in Fig. 1. The XRD and SEM images of an ilmenite sample are shown in Fig. 2. The average particle size of the ilmenite samples as received was around (100 ± 25) μm. Table 1 shows the metal oxide composition of the ilmenite sample analyzed by XRF. A series of leaching experiments under refluxing condition was conducted with different liquid-to-solid ratios of 85wt% H_3PO_4 and ilmenite. The white precipitate formed in the ilmenite/H_3PO_4 digestion mixture was confirmed as α-titanium bismonohydrogen orthophosphate monohydrate (TOP) with chemical formula $Ti(HPO_4)_2{\cdot}H_2O$ by the XRD analysis (curve (a) in Fig. 3); the result matches ICDD DB Card No. 01-080-1067. The FTIR spectrum further confirmed the formation of TOP [32–33]. The optimum ilmenite/phosphoric acid solid-to-liquid ratio was set to 1:8 (g/mL) on the basis of the maximum yield of the resulting TOP formed and the minimum residual weight of the unreacted ilmenite. Low solid-to-liquid ratios produced low weight percentages of TOP. The dry weights of TOP and unreacted ilmenite were measured after washing thoroughly with distilled water. The weight of the TOP precipitate reached the maximum level approximately after 5 h of refluxing. About 21 g of TiO_2 was obtained when 100 g of ilmenite was used as the starting material and the consumption levels of water and ammonia were 500 mL and 800 mL, respectively. The calculated recovery of titanium was about 35wt%–40wt% under the experimental conditions. A detailed description of the preparation of titanium phosphates from natural ilmenite was presented in a recent article [28].

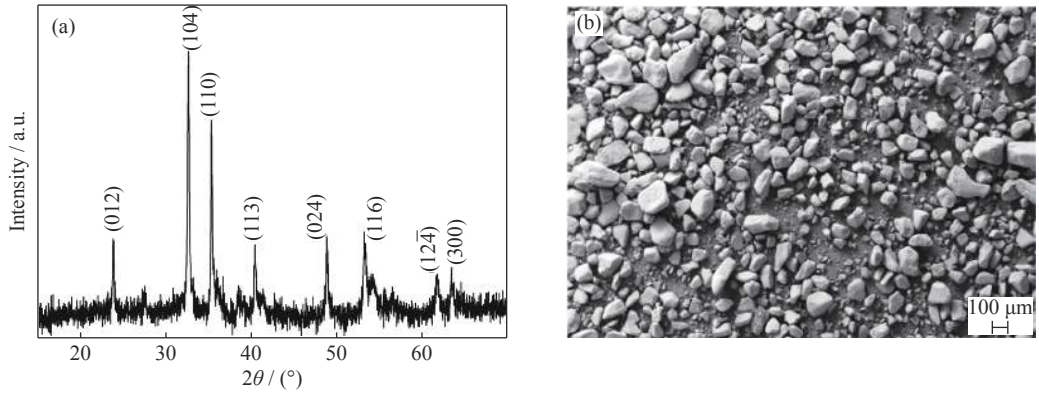

Fig. 2. (a) XRD pattern and (b) SEM image of ilmenite.

Table 1. Metal oxide composition of ilmenite and anatase TiO_2 wt%

Material	TiO_2	Fe as FeO	P as phosphates	CaO	SiO_2	SnO	ZnO	S as sulfates	MnO_2	ZrO_2	Nb_2O_5	Cr_2O_3	Al_2O_3
Ilmenite ($FeTiO_3$)	66.97	28.66	—	0.31	1.20	0.23	0.02	—	0.80	0.15	0.26	0.55	0.85
Anatase (TiO_2)	88.21	0.20	2.36	0.79	8.17	0.08	0.05	0.14	—	—	—	—	—

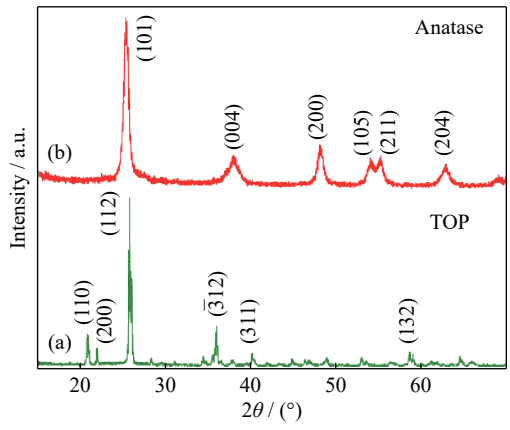

Fig. 3. XRD patterns of (a) TOP and (b) anatase TiO_2.

One of the key successes in the preparation of synthetic TiO_2 from ilmenite reported in this study is the preparation of an iron-free titanium phosphate compound, i.e., TOP, which can be used as a precursor for the preparation of anatase and rutile TiO_2. Titanium, in its 4+ oxidation state in natural ilmenite, is consumed during H_3PO_4 digestion for the formation of insoluble $Ti(HPO_4)_2{\cdot}H_2O$; whereas iron, in its 2+ oxidation state, leaches to the liquid phase to form the soluble $Fe(H_2PO_4)^+$ in concentrated H_3PO_4. Ratanatamskul *et al.* [34] reported that at pH < 3, H_3PO_4 with Fe(II) forms soluble $Fe(H_2PO_4)^+$ species as $H_2PO_4^-$ dominates in acidic conditions. Eq. (5) presents the formation of TOP and iron(II) phosphate complex.

$$FeTiO_3(s) + 10H^+(aq) + 3PO_4^{3-}(aq) \rightarrow Ti(HPO_4)_2 \cdot H_2O(s) + Fe(H_2PO_4)^+(aq) + 2H_2O(l) \quad (5)$$

The oxidation of Fe(II) to Fe(III) takes place at elevated temperatures, and highly soluble Fe(III) complexes are formed in concentrated H_3PO_4. Therefore, the leaching of iron from ilmenite into concentrated H_3PO_4 is not seriously problematic because of the formation of multiligand complexes of Fe(II)/(III) with phosphate, such as $Fe(H_2PO_4)^+$, $Fe(H_2PO_4)^{2+}$, $FeH_5(PO_4)_2^{2+}$, and $FeH_7(PO_4)^{3+}$, all of which are highly soluble in concentrated H_3PO_4 [34–37]. The chemical reaction for the iron dissolution and TOP precipitation in concentrated phosphoric acid can be proposed according to Eq. (5).

The current work did not attempt to understand the complexes of the iron phosphates that leached into phosphoric acid. The main focus was on the resulting solid fraction after acid digestion. Iron phosphates in H_3PO_4 liquor are used in many applications, such as in fertilizers, pesticides, and paint. To confirm iron leaching into H_3PO_4, this study conducted an experiment in which leachate was gradually added into cold acetone to obtain a white precipitate, which was isolated and calcined at 500°C for 5 h. The XRD pattern (not showm) confirmed that the material isolated was $Fe(PO_3)_3$; this result coincides with previously published work [38].

The white precipitate TOP, which was free of residual iron and H_3PO_4 after washing with distilled water, was reacted with ammonia (Eq. (6)) to obtain a precipitate of $Ti(OH)_4$. This precipitate was then thermally decomposed to form the final product TiO_2 (Eq. (7)).

$$Ti(HPO_4)_2 \cdot H_2O(s) + 4NH_4OH(aq) \rightarrow Ti(OH)_4 \cdot H_2O(s) \downarrow + 2(NH_4)_2HPO_4(aq) \quad (6)$$

$$Ti(OH)_4 \cdot H_2O(s) \xrightarrow{\Delta} TiO_2(s) + 3H_2O(l) \quad (7)$$

The removal of PO_4^{3-} from solid TOP reacted with ammonia increased the PO_4^{3-} concentration in the aqueous ammonia phase as $(NH_4)_2HPO_4$, resulting in the decrease of PO_4^{3-} in the solid phase. The concentration of PO_4^{3-} in the liquid phase was measured against the number of washes of solid TOP. The result clearly indicated that PO_4^{3-} concentration decreased with the number of washes. PO_4^{3-} reached undetectable levels after the fourth wash. The removal of PO_4^{3-} was the result of the formation of highly water-soluble ammonium phosphate salts in the presence of concentrated ammonia. Furthermore, the reaction of TOP with ammonia formed a fine white colloidal suspension, which consumed much time before settling down. The resulting suspension was a clear indication of the formation of titanium hydroxide. The calcination of this white precipitate for 5 h at 700°C developed a white powder characteristic of nano-level anatase TiO_2. The result was confirmed by XRD (curve (b) in Fig. 3) (ICDD DB Card No. 01-084-1285) analysis.

3.2. XRD and TEM analyses of TiO_2

The XRD patterns of the prepared TiO_2 samples were recorded after 5 h of calcination at temperatures of 500, 700, 800, and 900°C (Fig. 4). Curve (a) in Fig. 4 shows the XRD pattern of a sample calcined at 500°C. The result indicated the presence of the anatase phase with broad XRD peaks. At 700°C, the characteristic XRD peaks of anatase emerged with the 2θ values centered at 25.31°, 37.80°, 48.04°, 53.89°, 55.06°, and 62.69°, which corresponded to the crystal planes (101), (004), (200), (105), (211), and (204), respectively. The XRD pattern was in good agreement with that observed in the commercial anatase sample. The calculated particle sizes based on the Scherrer formula (Eq. (1)) [29] and the calculated anatase percentages based on the Spurr equation (Eq. (2)) [30] at different temperatures are summarized in Table 2. The calculated particle size for anatase at 700°C was 11.4 nm, and this value was further confirmed by the TEM images (Fig. 5) of the same sample. The XRD pattern obtained for the sample calcined at 800°C (curve (c) in Fig. 4) indicated the presence of rutile crystal planes (110), (101), (111), (211), and (220) corresponding to the 2θ values of 27.44°. 36.08°, 41.24°, 54.33°, and 56.64°, respectively, in addition to the typical anatase diffraction peaks. The presence of diffraction peaks that were characteristic of the anatase and rutile phases indicated that the phase transformation from anatase to rutile occurred at around 800°C. The calculated anatase percentage in the sample calcined at 800°C was approximately 70% (Table 2). The calculated particle size of TiO_2 at 800°C was 20.9 nm as the transformation to rutile was accompanied by a considerable grain growth [39]. A complete transition to rutile was evident at 900°C, at which point the characteristic XRD pattern for rutile emerged

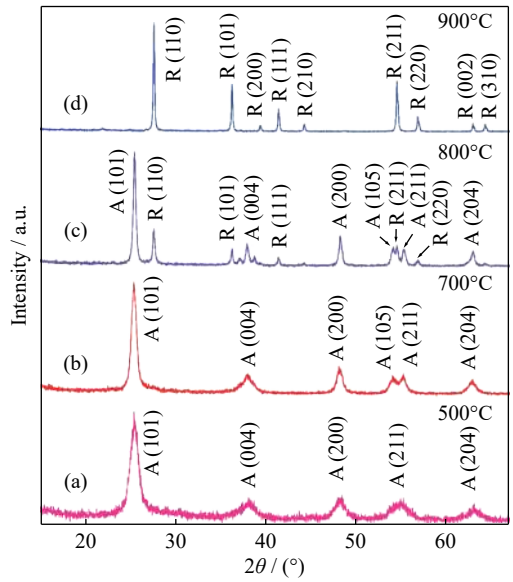

Fig. 4. XRD patterns of as-prepared TiO_2 samples calcined at different temperatures. A—Anatase; R—Rutile.

(curve (d) in Fig. 4). The temperature for the transition of anatase to rutile can be greatly affected by several factors, such as the presence of cationic and anionic impurities [40–41], grain size [42], and reaction atmosphere [43]. Furthermore, silica additives have been found to affect the anatase-to-rutile transition [44]. Therefore, the presence of a large amount of SiO_2 (~8%) in the synthesized anatase can primarily explain the high temperature for the anatase-to-rutile transition in this study. The calculated particle size of rutile was about 41.5 nm. Morphological characterization was performed by analyzing the TEM images of the prepared anatase TiO_2 samples (Fig. 5). The average particle size of the prepared anatase samples based on the TEM image analysis was in the (11 ± 4) nm range. Furthermore, the TEM images suggested that the TiO_2 nanoparticles exhibited a special shape.

Table 2. Particle size and anatase percentage calculated for the prepared TiO_2 samples at different calcination temperatures

Temperature / °C	Particle size / nm	Anatase / wt%
700	11.4	100
800	20.9	70
900	41.5	0

3.3. Raman analysis

Raman spectroscopy is a useful tool for the analysis of TiO_2 polymorphs as they exhibit characteristic Raman bands [7,45–46]. As the same fundamental structural units of [TiO_6] octahedron in rutile and anatase show different arrangements, these polymorphs belong to different space groups. Anatase belongs to the space group of $D_{4h}^{19} = I4_1/amd$ with $Z = 4$ and has the following irreducible representation for optical modes:

$$\Gamma_{\text{opt}} = A_{1g}(\text{R}) + 2B_{1g}(\text{R}) + 3E_g(\text{R}) + B_{2u}(\text{ia}) + A_{2u}(\text{IR}) + 2E_u(\text{IR}) \quad (8)$$

Therefore, anatase has six Raman active modes. Rutile belongs to the space group of $D_{4h}^{14} = P4_2/mnm$ with $Z = 2$ and has the following irreducible representation for optical modes:

$$\Gamma_{\text{opt}} = A_{1g}(\text{R}) + A_{2g}(\text{ia})_g + B_{1g}(\text{R}) + B_{2g}(\text{R}) + E_g(\text{R}) + A_{2u}(\text{IR}) + 2B_{1u}(\text{ia}) + 3E_u(\text{IR}) \quad (9)$$

Rutile has four Raman active modes. Curve (a) in Fig. 6 shows the Raman spectrum of anatase prepared after calcination at 700°C for 5 h. The Raman spectrum of anatase featured a strong and sharp band at 144 cm^{-1}; three mid-intensity bands at 396, 515, and 638 cm^{-1}; and a weak and low in-

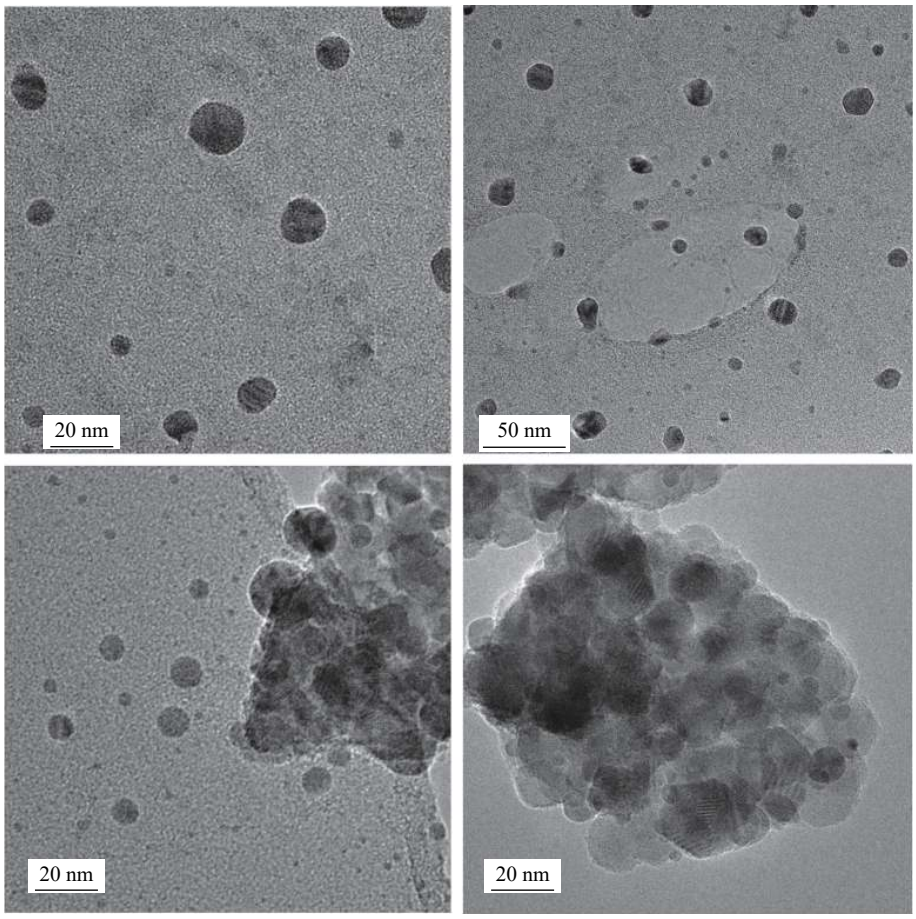

Fig. 5. HR-TEM images of anatase TiO_2 nanopowder calcined at 700°C at different magnifications.

tensity band at 197 cm^{-1}. The superposition of two fundamental bands at 515 cm^{-1} caused the appearance of six Raman bands for anatase that corresponded to the symmetries of E_g, E_g, B_{1g}, A_{1g}, B_{1g}, and E_g. The Raman spectrum of the prepared anatase is in good agreement with previously reported data [6,46]; hence, the chemical identity of the prepared anatase TiO_2 in the current work was successfully confirmed. As evident in the XRD analysis, a complete transformation of anatase to rutile occurred after calcination at 900°C for 5 h. Curve (b) in Fig. 6 shows the Raman spectrum of the prepared rutile sample. The sample featured two strong bands at 443 and 608 cm^{-1} and a weak band at 143 cm^{-1} corresponding to E_g, A_{1g}, and B_{1g}, respectively. The broad and mid-intensity peak at 238 cm^{-1} was attributed to the two-photon scattering of rutile. The XRD and Raman spectral data showed good mutual agreement and thus provide strong experimental evidence for the preparation of anatase and rutile from ilmenite/H_3PO_4 digestion.

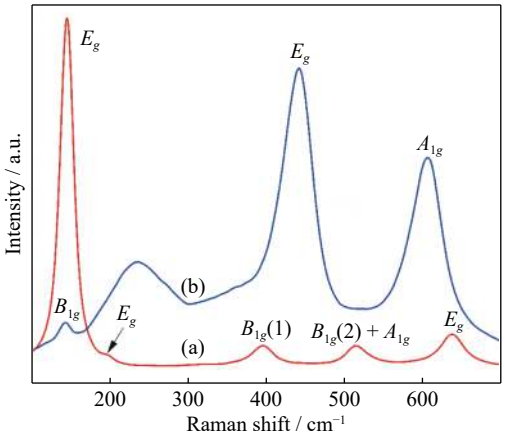

Fig. 6. Raman spectra of prepared (a) anatase and (b) rutile TiO_2 samples.

3.4. XRF analysis

The XRF analysis showed that the titanium oxide content increased to 88.21wt% (Ti metal basis of 90.60wt% in the prepared TiO_2 from 66.97wt% in ilmenite, as shown in Table 1). Trace metals Mn, Zr, Nb, Cr, and Al in ilmenite were absent in the final TiO_2. A low iron oxide content of 0.20wt% in the anatase samples further confirmed the effective removal of iron through the digestion of ilmenite with concentrated H_3PO_4. The presence of 2.36wt% phosphorous in phosphate form may be attributed to the insoluble metal phosphates, such as calcium and silicon phosphates [47], arising from H_3PO_4 digestion. In general, phosphoric acid (85wt%) has several anionic impurities [48], such as SO_4^{2-} and SiO_2^-. The presence of 0.14wt% sulfur, assumed to be in sulfate form in the final product, might have resulted from the phosphoric acid. Silicon, as an impurity in natural ilmenite and H_3PO_4, could be the main reason for the 8.17wt% silicon assumed to be in oxide form in the final product.

3.5. Optical properties

The UV–Vis DRS of the prepared anatase and rutile TiO_2 samples are shown in Fig. 7. The absorption edges for the anatase and rutile samples were located at 384 and 412 nm, respectively, in the UV–Vis absorption spectrum calculated from the diffuse reflectance data using the Kubelka–Munk method [31,49]. According to the literature [50], anatase is an indirect transition semiconductor, whereas rutile is a direct transition semiconductor. $[F(R) \times h\nu]^n$ was plotted as a function of photon energy, E_{phot} (inset of Fig. 7), to obtain the band gap energy corresponding to the value of E_{phot} extrapolated to $\alpha = 0$, where $F(R)$ is the Kubelka–Munk function. The calculated band gap energies of anatase and rutile were 3.09 and 2.95 eV, respectively. The values are within the range of the reported values in the literature [51–52]. However, the theoretical band gap values reported for anatase and rutile are 3.2 and 3.0 eV, respectively; these values are higher than those obtained for the prepared anatase and rutile. The presence of metallic and nonmetallic impurities (Table 1) in the final product may exert a significant effect on the shift of the band gap from the original value due to factors such as oxygen vacancy and lattice disorientations, which affect the electronic transition from the valence band to the conduction band [53]. For example, Karbassi *et al.* [54] reported that the presence of SiO_2 and Fe oxide in the TiO_2 matrix leads to the significant red shift of the optical response toward visible light owing to the reduced band gap energy.

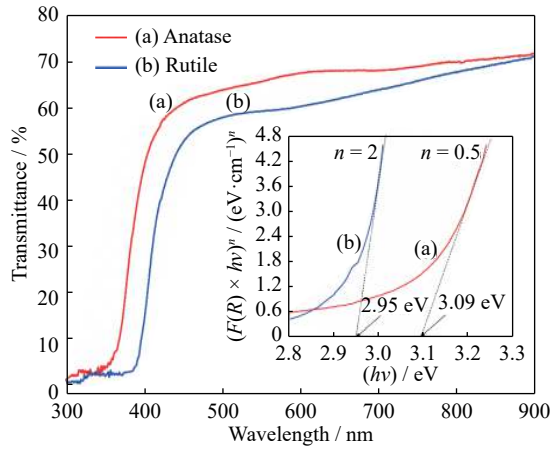

Fig. 7. UV–Vis DRS of (a) anatase and (b) rutile TiO_2 samples (inset: band gap curves).

3.6. Photocatalytic degradation of organic dyes

The photocatalytic properties of TiO_2 originate from the formation of photogenerated charge carriers (holes and electrons) generated after the absorption of ultraviolet (UV) light corresponding to the band gap. The photogenerated holes in

the valence band diffuse to the TiO_2 surface and react with adsorbed water molecules to form hydroxyl radicals. The photogenerated holes and hydroxyl radicals oxidize organic molecules adsorbed to the TiO_2 surface. Meanwhile, electrons in the conduction band also participate in reduction processes by reacting with molecular oxygen to produce superoxide radical anions. Superoxide radical ions are highly reactive and can subsequently breakdown the organic molecules present in a solution [55–58]. In the current work, the photodegradation kinetics of RhB for the TiO_2 and ilmenite samples were investigated by the pseudo first order method of the Langmuir–Hinshelwood model [59] (Eq. (8)), which is a well-established method for heterogeneous catalysis at low dye concentrations. According to this model,

$$\ln\left(\frac{C_0}{C_t}\right) = kt \tag{10}$$

where C_0 is the initial dye concentration, C_t is the dye concentration after UV irradiation time t, and k is the pseudo first order rate constant (min^{-1}). The k values were graphically determined using the regression method. Half-life, $t_{1/2}$, which is the time required to achieve a 50% reduction in dye concentration, was calculated by the following equation:

$$t_{1/2} = \frac{\ln 2}{k} = \frac{0.6931}{k} \tag{11}$$

The photocatalytic activities of the as-prepared anatase, rutile, and commercially available anatase and rutile samples on the degradation kinetics of RhB are shown in Fig. 8. The estimated rate constant k and $t_{1/2}$ (Eqs. (8) and (9), respectively) for the kinetic experiments are listed in Table 3.

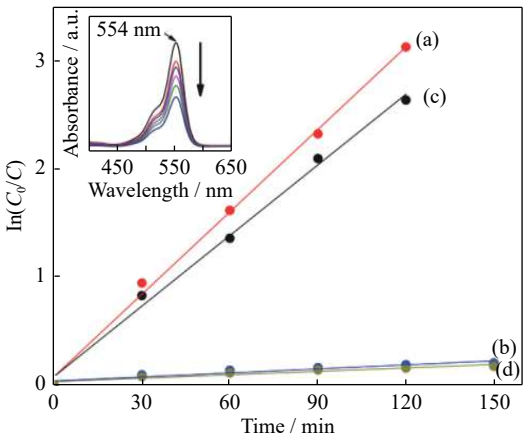

Fig. 8. Photocatalytic degradation kinetics of RhB dye over (a) prepared anatase, (b) prepared rutile, (c) commercial anatase, and (d) commercial rutile TiO_2 samples. Inset: UV–Vis absorption spectra at different time intervals for prepared anatase TiO_2.

The photobleaching of RhB was not observed in the control experiments performed using the starting material ilmenite in the presence and absence of UV light. Furthermore, the adsorption capacities were negligible across all samples, and the results are in agreement with previously published work [60]. The prepared and commercial anatase samples behaved almost identically for the RhB photodegradation because of their similar rate constants of 25.4×10^{-3} and 21.8×10^{-3} min^{-1}, respectively. Hence, the prepared anatase in this work exhibited the same photocatalytic potential as the commercial anatase used in these experiments. The rate constant of the as-prepared rutile was 1.24×10^{-3} min^{-1}, whereas that of the commercial rutile was 1.05×10^{-3} min^{-1}. The commercial and prepared rutile samples showed an average particle size close to 100 nm. In general, higher phase pure anatase exhibits high photocatalytic activity due to a large band gap and surface and charge transport properties [61]. The similar photodegradation kinetics observed in the prepared and commercial samples may be due to the low percentage of metallic impurities, such as iron, which could change the photobleaching rate. The presence of Si, P, and Ca impurities appeared to have no major influence on the kinetic parameters.

Table 3. Rate constant, $t_{1/2}$ and r^2 of degradation kinetics for RhB dye over TiO_2 samples

Material	k / (10^{-3} min^{-1})	$t_{1/2}$ / min	r^2
Anatase	25.4	27.3	0.9959
Rutile	1.24	559	0.8871
Commercial anatase	21.8	32.8	0.9934
Commercial rutile	1.05	660	0.8953

4. Conclusions

Anatase TiO_2 nanopowder was successfully prepared by employing a simple and novel ilmenite/H_3PO_4 digestion route. The precipitation of the iron-free titanium complex, i.e., TOP, in the H_3PO_4 leachate, which can be easily isolated from soluble iron in the form of iron–phosphate complexes, provides the key advantage of preparing a high-purity titanium precursor complex for anatase preparation. The repeated washing of TOP with ammonia not only formed titanium hydroxide but also removed the phosphate from the solid. The role of calcination temperature in the prepared anatase was investigated at 500–900°C, and the result showed that the anatase-to-rutile transformation occurred at above 700°C. The chemical identity of the prepared TiO_2 samples was confirmed by Raman and XRD data. The metal oxide content obtained via the XRF data indicated that the prepared TiO_2 samples had about 88wt% TiO_2. The photocatalytic performance of the as-prepared anatase and commercial anatase exhibited similar results on the photodegradation kinetics of RhB.

Acknowledgements

This work was financially supported by the University of

Sri Jayewardenepura under grant number ASP/01/RE/SCI/2019/31. The authors also thank Lanka Mineral Sands Ltd., Sri Lanka, for providing the ilmenite samples; the Central Instrument Facility of the University of Sri Jayewardenepura for the XRD sample analysis; and the Sri Lanka Institute of Nanotechnology Analytical Service for the Raman, TEM, and XRF analyses.

References

[1] A.F. Wells, *Structural Inorganic Chemistry*, Oxford University Press, Oxford, 2012.

[2] N.N. Greenwood and A. Earnshaw, *Chemistry of the Elements*, Elsevier Science, Amsterdam, 2012.

[3] X.Z. Ding, X.H. Liu, and Y.Z. He, Grain size dependence of anatase-to-rutile structural transformation in gel-derived nanocrystalline titania powders, *J. Mater. Sci. Lett.*, 15(1996), No. 20, p. 1789.

[4] K. Sabyrov, N.D. Burrows, and R.L. Penn, Size-dependent anatase to rutile phase transformation and particle growth, *Chem. Mater.*, 25(2013), No. 8, p. 1408.

[5] J.G. Li, T. Ishigaki, and X.D. Sun, Anatase, brookite, and rutile nanocrystals via redox reactions under mild hydrothermal conditions: Phase-selective synthesis and physicochemical properties, *J. Phys. Chem. C*, 111(2007), No. 13, p. 4969.

[6] D.A.H. Hanaor and C.C. Sorrell, Review of the anatase to rutile phase transformation, *J. Mater. Sci.*, 46(2011), No. 4, p. 855.

[7] G.A. Tompsett, G.A. Bowmaker, R.P. Cooney, J.B. Metson, K.A. Rodgers, and J.M. Seakins, The Raman spectrum of brookite, TiO_2 (*Pbca*, $Z = 8$), *J. Raman Spectrosc.*, 26(1995), No. 1, p. 57.

[8] J.S. Chen, Y.L. Tan, C.M. Li, Y.L. Cheah, D.Y. Luan, S. Madhavi, F.Y.C. Boey, L.A. Archer, and X.W. Lou, Constructing hierarchical spheres from large ultrathin anatase TiO_2 nanosheets with nearly 100% exposed (001) facets for fast reversible lithium storage, *J. Am. Chem. Soc.*, 132(2010), No. 17, p. 6124.

[9] X. Chen and S.S. Mao, Titanium dioxide nanomaterials: Synthesis, properties, modifications, and applications, *Chem. Rev.*, 107(2007), No. 7, p. 2891.

[10] A.L. Linsebigler, G. Lu, and J.T.J. Yates, Photocatalysis on TiO_2 surfaces: Principles, mechanisms, and selected results, *Chem. Rev.*, 95(1995), No. 3, p. 735.

[11] M.R. Hoffmann, S.T. Martin, W.Y. Choi, and D.W. Bahnemann, Environmental applications of semiconductor photocatalysis, *Chem. Rev.*, 95(1995), No. 1, p. 69.

[12] H.G. Yang, G. Liu, S.Z. Qiao, C.H. Sun, Y.G. Jin, S.C. Smith, J. Zou, H.M. Cheng, and G.Q. Lu, Solvothermal synthesis and photoreactivity of anatase TiO_2 nanosheets with dominant {001} facets, *J. Am. Chem. Soc.*, 131(2009), No. 11, p. 4078.

[13] D.P. Macwan, P.N. Dave, and S. Chaturvedi, A review on nano-TiO_2 sol–gel type syntheses and its applications, *J. Mater. Sci.*, 46(2011), No. 11, p. 3669.

[14] F. Bosc, A. Ayral, P.A. Albouy, and C.F. Guizard, A simple route for low-temperature synthesis of mesoporous and nanocrystalline anatase thin films, *Chem. Mater.*, 15(2003), No. 12, p. 2463.

[15] W.F. Sullivan and S.S. Cole, Thermal chemistry of colloidal titanium dioxide, *J. Am. Ceram. Soc.*, 42(1959), No. 3, p. 127.

[16] H.M. Cheng, J.M. Ma, Z.G. Zhao, and L.M. Qi, Hydrothermal preparation of uniform nanosize rutile and anatase particles, *Chem. Mater.*, 7(1995), No. 4, p. 663.

[17] G.S. Li, L.P. Li, J. Boerio-Goates, and B.F. Woodfield, High purity anatase TiO_2 nanocrystals: Near room-temperature synthesis, grain growth kinetics, and surface hydration chemistry, *J. Am. Chem. Soc.*, 127(2005), No. 24, p. 8659.

[18] C.C. Wang and J.Y. Ying, Sol−gel synthesis and hydrothermal processing of anatase and rutile titania nanocrystals, *Chem. Mater.*, 11(1999), No. 11, p. 3113.

[19] S. Cassaignon, M. Koelsch, and J.P. Jolivet, Selective synthesis of brookite, anatase and rutile nanoparticles: Thermolysis of $TiCl_4$ in aqueous nitric acid, *J. Mater. Sci.*, 42(2007), No. 16, p. 6689.

[20] R. Parra, M.S. Góes, M.S. Castro, E. Longo, P.R. Bueno, and J.A. Varela, Reaction pathway to the synthesis of anatase via the chemical modification of titanium isopropoxide with acetic acid, *Chem. Mater.*, 20(2008), No. 1, p. 143.

[21] W.S. Zhang, Z.W. Zhu, and C.Y. Cheng, A literature review of titanium metallurgical processes, *Hydrometallurgy*, 108(2011), No. 3, p. 177.

[22] K.K. Sahu, T.C. Alex, D. Mishra, and A. Agrawal, An overview on the production of pigment grade titania from titania-rich slag, *Waste Manage. Res.*, 24(2006), No. 1, p. 74.

[23] L. Palliyaguru, N.D.H. Arachchi, C.D. Jayaweera, and P.M. Jayaweera, Production of synthetic rutile from ilmenite via anion-exchange, *Miner. Process. Extr. Metall.*, 127(2018), No. 3, p. 169.

[24] T.A. Lasheen, Sulfate digestion process for high purity TiO_2 from titania slag, *Front. Chem. Eng. China*, 3(2009), No. 2, p. 155.

[25] T. Hisashi, N. Eiichi, T. Hitoshi, A. Masahiro, and O. Taijiro, Manufacture of high pure titanium(IV) oxide by the chloride Process. I. Kinetic study on leaching of ilmenite ore in concentrated hydrochloric acid solution, *Bull. Chem. Soc. Jpn*, 55(1982), No. 6, p. 1934.

[26] S. Sariman, Y.K. Krisnandi, and B. Setiawan, Anatase TiO_2 enrichment from bangka ilmenite ($FeTiO_3$) and its photocatalytic test on degradation of congo red, *Adv. Mater. Res.*, 789(2013), p. 538.

[27] S. Wahyuingsih, A.H. Ramelan, E. Pramono, A.D. Sulistya, P.R. Argawan, F.D. Dharmawan, L. Rinawati, Q.A. Hanif, E. Sulistiyono, and F. Firdiyono, Synthesis of anatase and rutile TiO_2 nanostructures from natural ilmenite, *AIP Conf. Proc.*, 1710(2016), No. 1, art. No. 030023.

[28] L. Palliyaguru, M.U.S. Kulathunga, K.G.U.R. Kumarasinghe, C.D. Jayaweera, and P.M. Jayaweera, Facile synthesis of titanium phosphates from ilmenite mineral sand: Potential white pigments for cosmetic applications, *J. Cosmet. Sci.*, 70(2019), No. 3, p. 149.

[29] B.D. Cullity, *Elements of X-ray Diffraction*, 3rd ed., Addison-Wesley Publishing Company, New Jersey, 1978.

[30] R.A. Spurr and H. Myers, Quantitative analysis of anatase–rutile mixtures with an X-ray diffractometer, *Anal. Chem.*, 29(1957), No. 5, p. 760.

[31] P. Kubelka, New contributions to the optics of intensely light-scattering materials. Part I, *J. Opt. Soc. Am.*, 38(1948), No. 5, p. 448.

[32] A. Stoch, W. Jastrzębski, A. Brożek, J. Stoch, J. Szaraniec, B. Trybalska, and G. Kmita, FTIR absorption–reflection study of biomimetic growth of phosphates on titanium implants, *J. Mol. Struct.*, 555(2000), No. 1-3, p. 375.

[33] T.S. Sysoeva, E.A. Asabina, V.I. Pet'kov, and V.S. Kur-

azhkovskaya, Alkali (alkaline-earth) metal, aluminum, and titanium complex orthophosphates: Synthesis and characterization, *Russ. J. Inorg. Chem.*, 54(2009), No. 6, p. 829.

[34] C. Ratanatamskul, S. Chintitanun, N. Masomboon, and M.C. Lu, Inhibitory effect of inorganic ions on nitrobenzene oxidation by fluidized-bed Fenton process, *J. Mol. Catal. A*: *Chem.*, 331(2010), No. 1, p. 101.

[35] T.B. Zhang, Y.C. Lu, and G.S. Luo, Effects of temperature and phosphoric acid addition on the solubility of iron phosphate dihydrate in aqueous solutions, *Chin. J. Chem. Eng.*, 25(2017), No. 2, p. 211.

[36] J.J. Beltrán, F.J. Novegil, K.E. García, and C.A. Barrero, On the reaction of iron oxides and oxyhydroxides with tannic and phosphoric acid and their mixtures, *Hyperfine Interact.*, 195(2010), No. 1, p. 133.

[37] M. Iuliano, L. Ciavatta, and G. De Tommaso, On the solubility constant of strengite, *Soil Sci. Soc. Am. J.*, 71(2007), No. 4, p. 1137.

[38] W.J. Zhou, W. He, X.D. Zhang, J.A. Liu, Y. Du, S.P. Yan, X.Y. Tian, X.A. Sun, X.X. Han, and Y.Z. Yue, Simple and rapid synthesis of $Fe(PO_3)_3$ by microwave sintering, *J. Chem. Eng. Data*, 54(2009), No. 7, p. 2073.

[39] Y.H. Zhang and A. Reller, Phase transformation and grain growth of doped nanosized titania, *Mater. Sci. Eng. C*, 19(2002), No. 1, p. 323.

[40] W.F. Sullivan and J.R. Coleman, Effect of sulphur trioxide on the anatase–rutile transformation, *J. Inorg. Nucl. Chem.*, 24(1962), No. 6, p. 645.

[41] J. Yang and J.M.F. Ferreira, On the titania phase transition by zirconia additive in a sol–gel-derived powder, *Mater. Res. Bull.*, 33(1998), No. 3, p. 389.

[42] A.A. Gribb, and J.F. Banfield, Particle size effects on transformation kinetics and phase stability in nanocrystalline TiO_2, *Am. Mineral.*, 82(1997), No. 7-8, p. 717.

[43] K.J.D. Mackenzie, The calcination of titania. VI. The effect of reaction atmosphere and electric fields on the anatase–rutile transformation, *Trans. J. Brit. Ceram. Soc.*, 74(1975), No. 4, p. 121.

[44] K. Okada, N. Yamamoto, Y. Kameshima, A. Yasumori, and K.J.D. MacKenzie, Effect of silica additive on the anatase-to-rutile phase transition, *J. Am. Ceram. Soc.*, 84(2001), No. 7, p. 1591.

[45] Y.H. Zhang, C.K. Chan, J.F. Porter, and W. Guo, Micro-Raman spectroscopic characterization of nanosized TiO_2 powders prepared by vapor hydrolysis, *J. Mater. Res.*, 13(2011), No. 9, p. 2602.

[46] T. Ohsaka, F. Izumi, and Y. Fujiki, Raman spectrum of anatase, TiO_2, *J. Raman Spectrosc.*, 7(1978), No. 6, p. 321.

[47] E.O. Huffman, W.E. Cate, M.E. Deming, and K.L. Elmore, Solubility of phosphates, rates of solution of calcium phosphates in phosphoric acid solutions, *J. Agric. Food Chem.*, 5(1957), No. 4, p. 266.

[48] W.E. Cate and M.E. Deming, Effect of impurities on density and viscosity of simulated wet-process phosphoric acid, *J. Chem. Eng. Data*, 15(1970), No. 2, p. 290.

[49] A. Hagfeldt and M. Graetzel, Light-induced redox reactions in nanocrystalline systems, *Chem. Rev.*, 95(1995), No. 1, p. 49.

[50] J.F. Zhang, P. Zhou, J.J. Liu, and J.G. Yu, New understanding of the difference of photocatalytic activity among anatase, rutile and brookite TiO_2, *Phys. Chem. Chem. Phys.*, 16(2014), No. 38, p. 20382.

[51] N. Serpone, Is the band gap of pristine TiO_2 narrowed by anion- and cation-doping of titanium dioxide in second-generation photocatalysts? *J. Phys. Chem. B*, 110(2006), No. 48, p. 24287.

[52] K. Madhusudan Reddy, S.V. Manorama, and A. Ramachandra Reddy, Bandgap studies on anatase titanium dioxide nanoparticles, *Mater. Chem. Phys.*, 78(2003), No. 1, p. 239.

[53] E.M. Samsudin and S.B. Abd Hamid, Effect of band gap engineering in anionic-doped TiO_2 photocatalyst, *Appl. Surf. Sci.*, 391(2017), p. 326.

[54] M. Karbassi, A. Nemati, M.H. zari, and K. Ahadi, Effect of iron oxide and silica doping on microstructure, bandgap and photocatalytic properties of titania by water-in-oil microemulsion technique, *Trans. Indian Ceram. Soc.*, 70(2011), No. 4, p. 227.

[55] J. Schneider, M. Matsuoka, M. Takeuchi, J.L. Zhang, Y. Horiuchi, M. Anpo, and D.W. Bahnemann, Understanding TiO_2 photocatalysis: Mechanisms and materials, *Chem. Rev.*, 114(2014), No. 19, p. 9919.

[56] S.G. Kumar and L.G. Devi, Review on modified TiO_2 photocatalysis under UV/visible light: Selected results and related mechanisms on interfacial charge carrier transfer dynamics, *The J. Phys. Chem. A*, 115(2011), No. 46, p. 13211.

[57] C.S. Turchi and D.F. Ollis, Photocatalytic degradation of organic water contaminants: Mechanisms involving hydroxyl radical attack, *J. Catal.*, 122(1990), No. 1, p. 178.

[58] C. Naccache, P. Meriaudeau, M. Che, and A.J. Tench, Identification of oxygen species adsorbed on reduced titanium dioxide, *Trans. Faraday Soc.*, 67(1971), No. 67, p. 506.

[59] W.Z. Tang and A.N. Huren, UV/TiO_2 photocatalytic oxidation of commercial dyes in aqueous solutions, *Chemosphere*, 31(1995), No. 9, p. 4157.

[60] J. He,Y.E. Du,Y. Bai, J. An, X.M. Cai, Y.Q. Chen, P.F. Wang, X.J. Yang and Q. Feng, Facile formation of anatase/rutile TiO_2 nanocomposites with enhanced photocatalytic activity, *Molecules*, 24(2019), No. 16, p. 2996.

[61] T. Luttrell, S. Halpegamage, J.G. Tao, A. Kramer, E. Sutter, and M. Batzill, Why is anatase a better photocatalyst than rutile? - Model studies on epitaxial TiO_2 films, *Sci. Rep.*, 4(2014), art. No. 4043.